Nucleic Acids Research, 2004, Vol. 32, No. 10 **2977–2986**
DOI: 10.1093/nar/gkh628

DnaG interacts with a linker region that joins the N- and C-domains of DnaB and induces the formation of 3-fold symmetric rings

Jenny Thirlway, Ian J. Turner[1], Christopher T. Gibson[1], Laurence Gardiner, Kevin Brady, Stephanie Allen[1], Clive J. Roberts[1] and Panos Soultanas*

Centre for Biomolecular Sciences (CBS) and [1]Laboratory of Biophysics and Surface Analysis (LBSA), School of Pharmacy, University of Nottingham, University Park, Nottingham NG7 2RD, UK

Received April 8, 2004; Revised and Accepted May 11, 2004

ABSTRACT

Loading of the replicative ring helicase onto the origin of replication (*ori*C) is the final outcome of a well coordinated series of events that collectively constitute a primosomal cascade. Once the ring helicase is loaded, it recruits the primase and signals the switch to the polymerization mode. The transient nature of the helicase–primase (DnaB–DnaG) interaction in the *Escherichia coli* system has hindered our efforts to elucidate its structure and function. Taking advantage of the stable DnaB–DnaG complex in *Bacillus stearothermophilus*, we have reviewed conflicting mutagenic data from other bacterial systems and shown that DnaG interacts with the flexible linker that connects the N- and C-terminal domains of DnaB. Furthermore, atomic force microscopy (AFM) imaging experiments show that binding of the primase to the helicase induces predominantly a 3-fold symmetric morphology to the hexameric ring. Overall, three DnaG molecules appear to interact with the hexameric ring helicase but a small number of complexes with two and even one DnaG molecule bound to DnaB were also detected. The structural/functional significance of these data is discussed and a speculative structural model for this complex is suggested.

INTRODUCTION

DNA helicases are motor proteins that couple the hydrolysis of nucleotide triphosphates (NTPs) to DNA unwinding (1–3). This basic unwinding activity is crucial in almost all aspects of nucleic acid metabolism, including DNA replication and repair. The hexameric DnaB protein is the most important bacterial helicase, as it is the main replicative DNA helicase associated with the replisome during DNA replication (4). It is a remarkable protein in the sense that it acts as a 'docking' protein interacting with different partners and modulating a variety of different functions. The ever-increasing list of DnaB-interacting proteins includes the bacterial replication initiator protein DnaA (5), the plasmid replication initiator proteins RepA and π (6), the bacteriophage replication initiator protein λP (7), the helicase loaders DnaC (8,9) and DnaI (10,11) in Gram-negative and Gram-positive bacteria, respectively, the B subunit of DNA gyrase GyrB (12), the central organizer of the DNA polymerase clamp-loader DnaX (13–15), the DNA replication termination proteins Rtp and Tus in Gram-negative and Gram-positive bacteria, respectively (16,17) and the bacterial primase DnaG (18,19). Loading of a ring helicase onto DNA is a complicated process that is mediated by the ordered stepwise action of a primosomal cascade of proteins. This in turn recruits the primase DnaG onto the origin of replication *ori*C (20–22). The helicase–primase interaction signifies the completion of primosomal assembly and switch to polymerization. To date little is known about the molecular and structural details of the helicase–primase interaction.

Mutagenesis studies in the *Escherichia coli* (23) and *Salmonella typhimurium* (24,25) DnaB proteins, in combination with indirect biochemical assays, implicated five residues in this interaction. The equivalent residues are also conserved in *Bacillus stearothermophilus* DnaB (E15, Y88, I119, I125 and L138) (26). Other studies suggested that different distant residues are involved, since two double DnaB mutants (D212A-D213A and K216A-K217A) were reported to be defective in DnaG-binding, as assayed by an enzyme-linked immunosorbent assay (27). The equivalent residues in *B.stearothermophilus* DnaB (T191-E192 and R195-M196) are not conserved and reside in the C-terminal domain (26). Overall, these results suggest that different regions residing on the N- and C-domains of DnaB are involved in its interaction with the primase. Structural information on DnaB is limited to the small N-terminal domain (28,29), and the absence of a complete structure for the intact hexamer makes it difficult to obtain a detailed insight into the molecular mechanisms that underpin this interaction. Recent crystal structures of the T7 gene 4 helicase (30,31), and RepA (32) proteins that exhibit some homology to DnaB offer us the opportunity to re-examine the structural features that mediate the DnaB–DnaG interaction.

In the *E.coli* system, the helicase–primase complex is not stable enough *in vitro* to enable its physical isolation and

*To whom correspondence should be addressed. Tel: +44 115 9513525; Fax: +44 115 9513564; Email: panos.soultanas@nottingham.ac.uk

purification. In the *B.stearothermophilus* system a stable complex can be isolated, providing a direct assay for this interaction (19). We took advantage of this property and employed site-directed mutagenesis to resolve the controversial issue of mapping the important DnaB amino acid residues involved in this interaction. Employing amino acid sequence comparisons and structural modelling based upon the T7 gp4 and RepA structures, we targeted the equivalent amino acid residues of the *B.stearothermophilus* DnaB protein. Using a combination of mutagenesis, biochemical analysis and protease protection studies, we show that DnaG interacts mainly across a flexible linker region of DnaB that connects the N- and C-terminal domains. DnaG also makes contacts with residues in the N-terminal domain that may modulate the affinity of this interaction in response to other replisomal proteins binding to DnaB. Our atomic force microscopy (AFM) imaging of the complex was not of high enough spatial resolution to resolve individual proteins within the complex, but has revealed that the complex adopts a 3-fold symmetric ring structure, allowing us to suggest a speculative model for its architecture based upon our data and also data from other groups on the dynamics of the DnaB ring.

MATERIALS AND METHODS

Site-directed mutagenesis

Site-directed mutagenesis was carried out by PCR, as described elsewhere (33), using appropriate mutagenic oligonucleotides (Supplementary Material), together with the forward (5′-GCAAGGAATGGTGCATGCAAGGAG-3′) and reverse (5′-CTCGAGTGCGGCCGCAAGCTTGTC-3′) cloning primers. All mutant genes were cloned as NdeI–HindIII fragments in pET22b (Novagen). All mutations as well as the absence of other spurious mutations were verified by sequencing.

Protein purification

Wild-type and mutant DnaB proteins were overexpressed in BL21 (DE3) *E.coli* and purified by a combination of Blue Sepharose, MonoQ, Hi-Trap heparin and Superdex S-200 gel filtration chromatography following the same protocol as described previously (19,33). DnaG and P16 were purified by a combination of Hi-Trap heparin, Source-Q and Superdex S-75 gel filtration chromatography, as described elsewhere (19). All proteins were >98% pure as assessed by SDS–PAGE analysis (data not shown). Protein concentrations were determined spectrophotometrically using specific absorbance values at 280 nm of 0.418 and 0.66 for DnaB and DnaG proteins, respectively. The only exception was the Y88A mutant whose specific absorbance was 0.394. All specific absorbance values were calculated using the formula

$$A_{280}\ (1\ \text{mg/ml}) = (5690W + 1280Y + 120C)/M$$

where W, Y and C are the numbers of Trp, Tyr and Cys residues in a polypeptide of mass M, and 5690, 1280 and 120 are the respective extinction coefficients for these residues. All mutant proteins were chromatographically stable and exhibited normal oligomerization states (hexamers) at either low (100–250 mM NaCl) or high (500 mM NaCl) ionic strength conditions compared with the wild-type DnaB protein.

Analytical gel filtration

Wild-type or mutant DnaB was mixed with DnaG in 0.5 ml TED [50 mM Tris pH 7.4, 1 mM EDTA, 1 mM dithiothreitol (DTT)] including 100, 250 or 500 mM NaCl and in a molar ratio of 0.5 μM DnaB (referring to hexamer) to 3 μM DnaG (referring to monomer). The mixtures were equilibrated on ice for 15 min prior to loading onto a Superdex S-200 10/30 (Amersham Pharmacia Biotech) gel filtration column, equilibrated in the same buffer (TED plus 100, 250 or 500 mM NaCl, as appropriate). Gel filtration was carried out at 0.5 ml/min and 0.5 ml fractions were collected. Samples from the peaks were analysed by SDS–PAGE and gels were stained by silver staining or a Coomassie BioSafe stain (Bio-Rad).

ATPase assays

The DNA-independent ATPase activity of wild-type and mutant DnaB proteins was assayed by monitoring NADH oxidation, as described before (11,33,34). Briefly, reactions were carried out in 20 mM Tris pH 7.5, 50 mM NaCl, 10 mM $MgCl_2$, 5 mM DTT and 100 nM DnaB (referring to hexamer), in the presence or absence of 400 nM DnaG, at varying ATP concentrations in a total volume of 1 ml. The reaction was initiated by addition of the helicase (or helicase–primase mixture). All the ATPase reaction profiles shown represent the averages of three independent experiments. The *B.stearothermophilus* DnaB protein does not exhibit first-order Michaelis–Menten kinetics. Instead, the ATPase profile exhibits a characteristic curve attributed to cooperative allosteric effects within the hexamer (11,19,33). No quantitative parameters can be derived and our comparisons of ATPase activities are merely qualitative.

Helicase assays

Helicase assays were carried out as described elsewhere (33).

Yeast two-hybrid (Y2H) experiments

Y2H experiments were carried out using the MATCHMAKER Two-Hybrid system 2 (Clontech). The *dnaG* gene was cloned as an NcoI–XhoI fragment into pACT2, while DnaB, P17 (N-terminal domain of DnaB) and P33 (C-terminal domain of DnaB) were cloned as NcoI–XhoI fragments into the NcoI–SalI sites of pAS2-1. The positive control is based upon the p53-SV40 T antigen interaction. It has the pVA3-1 plasmid carrying the GAL4 DNA binding domain fused to murine p53 and a *trp* nutritional selection marker, together with the pTD1 plasmid carrying the GAL4 activation domain fused to the SV40 large T antigen and a *leu* nutritional selection marker. The negative control shows that there is no interaction between DnaB and SV40 large T antigen, using the pAS2-1-DnaB and pTD1 plasmids described above. All plasmids were transformed into yeast by electroporation (35) and the detection of positive interactions was carried out by the agarose overlay method (36).

Limited proteolysis

Limited proteolysis was carried out in 50 mM Tris pH 7.4, 2 mM EDTA, 100 mM NaCl, 10% (v/v) glycerol and 1 mM

DTT, using a molar ratio of 1:5000 for papain:DnaB and 1:100 for trypsin:DnaB, in the presence or absence of a large excess of P16 for 25 min at 37°C. DnaB and P16 mixtures were incubated for 15 min on ice prior to the addition of the protease. Samples were removed at 5 min intervals and quenched by addition of gel loading buffer [50 mM Tris pH 6.8, 100 mM DTT, 2% (w/v) SDS, 10% glycerol, 0.1% bromophenol blue] and heating at 94°C for 5 min. Protein fragments were resolved by SDS–PAGE through a 15% polyacrylamide gel and visualized by Coomassie staining.

AFM imaging

The DnaB–DnaG complex was formed by mixing DnaB with a six molar excess of DnaG (referring to hexamers of DnaB and monomers of DnaG) and separating the complex from excess unbound DnaG by gel filtration through an analytical Superdex S200 gel filtration column (Amersham Pharmacia Biotech) in 50 mM Tris pH 7.4 and 1 mM EDTA (19). DnaB and DnaG samples were buffer exchanged in the same buffer for imaging. Protein samples were typically diluted to between 10 and 85 μg/ml in the same buffer and samples of 5–10 μl were incubated with freshly cleaved mica (Agar Scientific, Stansted, UK) for 2–10 s, rinsed with 5 ml of distilled H_2O and allowed to dry under a gentle flow of nitrogen gas. AFM was conducted in air at room temperature, with a scanning rate typically between 2 and 3 Hz in tapping mode using a Nanoscope IIIa with a type E scanner (Veeco, Cambridge, UK). The cantilevers used were silicon tapping probes with a spring constant of 34.4–74.2 N/m (Olympus, OMCL-AC160TS). The tapping set-point was adjusted to minimize probe–sample interactions. Images were recorded in both topography and phase modes with a pixel size of 512 × 512, flattened and analysed with WSxM software 3.0 Beta 2.3 (Nanotec Electronica S.L, Spain). All the figures presented show data obtained with topography mode. The globular subunits that constituted 3-fold symmetric rings were analysed systematically. Cross-hairs were drawn in each sphere in the *X* and *Y* directions, and measurements were done at half-height using the line-measurement feature on the SPIP metrology software package (Image Metrology A/S, Lyngby, Denmark). The size of DnaG was also determined in a similar manner from samples consisting only of DnaG. For the DnaB–DnaG samples, subunits ⩽20 nm were classed as unbound DnaB and larger features as bound DnaB–DnaG. This threshold was selected based on the lower limit in the spread of the complexes. Three distinct subpopulations ($DnaB_6$–$DnaG_3$, $DnaB_6$–$DnaG_2$ and $DnaB_6$–$DnaG_1$) were observed for which the means and s.d. values were also determined. For the $DnaB_6$–$DnaG_2$ and $DnaB_6$–$DnaG_1$ subpopulations, the bound and unbound subunits were analysed separately.

RESULTS

Mutations in the N-domain and interdomain linker region of DnaB

Amino acid residues E15, Y88 and I119 are conserved between *E.coli* and *B.stearothermophilus* DnaB proteins. From the crystal (28) and solution (29) structures of the N-terminal domain of *E.coli* DnaB it is apparent that they are all clustered on the surface of the protein relatively close to each other, forming a potential DnaG interacting 'pocket'. (Supplementary Material). I119 is the last residue of a helix at the C-terminal end of the domain. A flexible linker extending from this position joins the N-domain with the RecA-like C-domain. I125 and L138 are in this flexible linker region and are not visible in these structures. Mutations at these positions were investigated by gel filtration of mutant DnaB–DnaG complexes and examination of the effects in DnaB ATPase and helicase stimulation by DnaG *in vitro* (19,33).

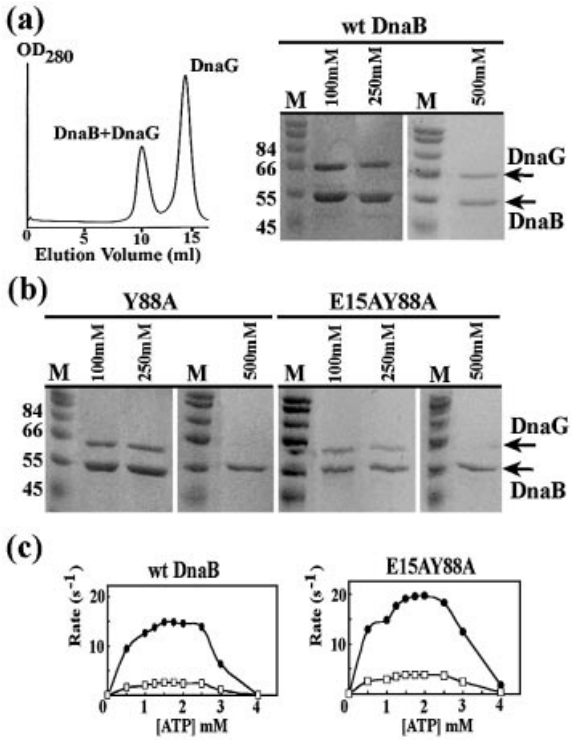

Figure 1. Mutations in the N-domain of DnaB affect DnaG binding at high ionic strength conditions. (**a**) Wild-type DnaB forms a stable complex with DnaG at 100, 250 and 500 mM NaCl that can be isolated by gel filtration. A representative gel filtration profile for the wtDnaB + DnaG mixture is shown. The presence of both proteins in the complex was verified by SDS–PAGE analysis of samples from the early peak that contains the complex. Arrows indicate the positions of the two proteins in the gel. Excess DnaG elutes later from the column. (**b**) Both Y88A and E15AY88A mutant DnaB proteins formed a stable complex with DnaG at 100 and 250 mM NaCl, but the complex dissociated at 500 mM NaCl. SDS–PAGE analysis of samples from the early peak revealed the dissociation of DnaG from the hexameric DnaB at 500 mM NaCl. (**c**) The ATPase activity of E15AY88A was stimulated by DnaG in a manner similar to that of the wild-type DnaB under the low ionic strength conditions of our assay. Open squares indicate the ATPase activity profile of DnaB alone whereas filled circles represent that of DnaB in the presence of excess DnaG.

E15 and Y88 are conserved in *E.coli* DnaB (E32 and Y105) and have been implicated in the primase interaction by indirect *in vitro* reconstituted rolling circle replication assays (23). Our E15A (data not shown) and Y88A point mutants both formed stable complexes with DnaG under low ionic strength conditions, similarly to the wild-type DnaB (Fig. 1a and b). These complexes were functional, since the ATPase and helicase activities of both mutants were stimulated by DnaG under the low ionic strength conditions of our assays (data not shown). Interestingly, the Y88A mutant could not form a stable complex with DnaG at 500 mM NaCl (Fig. 1b), whereas

both the wild-type DnaB (Fig. 1a) and the E15A mutant (data not shown) could form stable complexes with DnaG.

The E15A-Y88A double mutant behaved in a similar manner to the Y88A point mutant, forming a stable complex with DnaG at low ionic strength (Fig. 1b) but not at high ionic strength (Fig. 1b). There was no cumulative defect due to the additional E15A mutation. Again, the complex was functional, as DnaG stimulated the ATPase (Fig. 1c) and helicase (data not shown) activities of the E15A-Y88A double mutant under the low ionic strength conditions of our assays. We were unable to investigate these activities under high ionic conditions as the interaction of ATP with DnaB was impaired, manifested by reduced activities of the wild-type DnaB at 500 mM NaCl (data not shown). The cumulative data suggest that Y88 is involved in the interaction of DnaB with DnaG in a subtle manner, whereas E15 is not.

Elegant studies by Marian's group revealed that E32K (equivalent to E15) and Y105A (equivalent to Y88) point mutations in *E.coli* DnaB resulted in longer Okazaki fragments in reconstituted rolling circle replication assays, a consequence of altered affinities for DnaG rather than alterations in the rate of replication fork progression (23). Interestingly, the E32A mutant did not exhibit a detectable defect, in agreement with our results. Furthermore, these mutants exhibited differential defects in general priming that were also manifested in replication forks reconstituted only in the presence of DnaB, DnaC and DnaG. Therefore E32 and Y105 were proposed to act as allosteric residues mediating the effects of either SSB and/or one of the polymerase subunits on the helicase–primase interaction within the replication fork. DnaB interacts exclusively with the τ (DnaX) subunit of the DNA polymerase III holoenzyme (13–15) and *in vitro* forms a stable triple complex with DnaG and τ (data not shown). The E15AY88A double mutant also formed a triple complex, suggesting that these residues are unlikely to participate in any τ-mediated allosteric effects on the helicase–primase interaction. These data show that the conserved E and Y residues do not contribute the major binding energy for the formation of the helicase–primase complex in the absence of other proteins and are unlikely to mediate DNA polymerase allosteric effects, but could instead have a more subtle effect on its stability.

On the other hand, the ability of both I119A and I125A point mutants to form stable complexes with DnaG was impaired at low and high ionic strengths (Fig. 2a and b). This was also evident by the inability of DnaG to stimulate significantly their ATPase and helicase activities (Fig. 2c). The L138A mutant was unaffected and formed a stable complex with DnaG at low and high ionic strengths, while DnaG stimulated its ATPase and helicase activities (data not shown). Interestingly, the ATPase activity profiles of I119A and I125A were different to those of the wild type and the E15A, Y88A, E15AY88A mutants. Whereas the latter exhibited the characteristic non-linear profile with a maximum between 1.5 and 1.75 mM ATP (Fig. 1c) (19,33), the former exhibited different profiles with maxima shifted to around 1 mM ATP (Fig. 3). Thus linker mutations subtly affect the ATPase activity of DnaB. Similar results were observed in the *E.coli* DnaB where mutations at the equivalent I135 and I141 residues also affected the DNA-independent and ssDNA-stimulated ATPase activities (25). Relative repositioning of

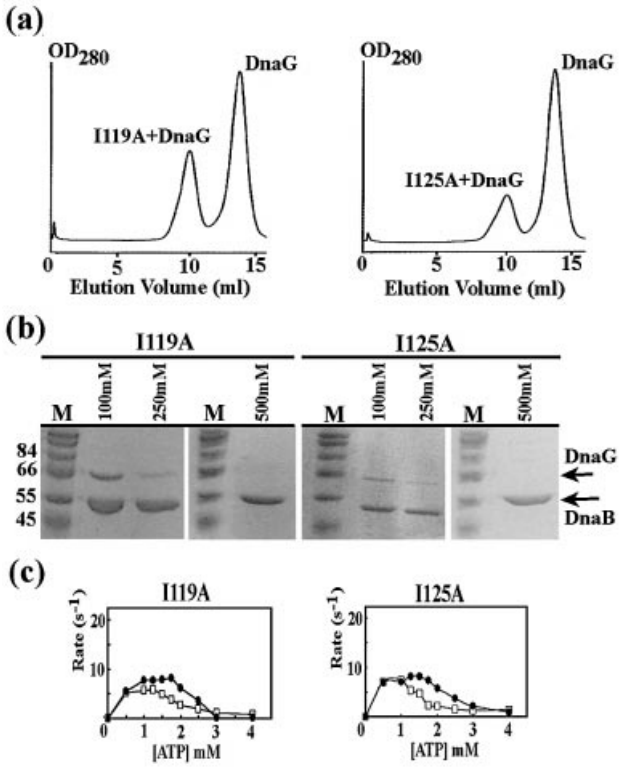

Figure 2. Mutations in the linker region of DnaB affect DnaG binding even at low ionic strength conditions. (**a**) Representative gel filtration profiles of I119A+DnaG and I125A+DnaG mixtures. (**b**) SDS–PAGE gels of samples from the early peak verifying the dissociation of DnaG from the hexameric DnaB at 250 and 500 mM NaCl and the very small amount of DnaG that remains bound to DnaB at 100 mM NaCl. Arrows indicate the positions of the two proteins in the gels. (**c**) The ATPase activities of the I119A and I125A DnaB mutants are not stimulated significantly by the presence of excess DnaG in the reaction mixture. Open squares indicate the ATPase activity profile of DnaB alone whereas solid circles represent that of DnaB in the presence of excess DnaG.

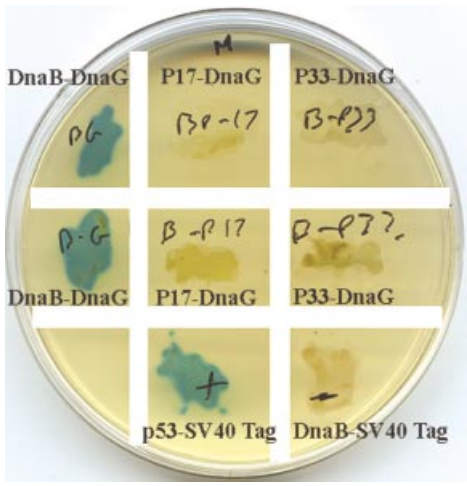

Figure 3. The DnaB–DnaG interaction assayed by Y2H. Y2H experiments indicate a strong interaction signal between DnaB and DnaG but no signals for either the N-domain (P17) or the C-domain (P33) of DnaB and DnaG. The positive control indicates an interaction between p53 and the SV40 large T antigen and the negative control indicates no interaction between DnaB and p53. Two separate clones were tested for each interaction.

the N-domains, potentially affecting the primase-binding site, was suggested to explain the inability of these mutants to interact with DnaG. This is an attractive hypothesis and predicts that the N-domains can somehow affect the ATPase activity of the C-domains within the hexamer. Several indirect pieces of evidence reinforce this notion. The N-domains affect correct oligomerization (19,37) and the C-domains have a different ATPase profile compared with the full-length *B.stearothermophilus* DnaB protein (11,19). Three N-domains have been shown to interact with adjacent C-domains within 3-fold symmetric hexamers compared with adjacent N-domains within 6-fold symmetric hexamers, thus offering a likely means of allosteric communication between N- and C-domains around the hexamer (38).

Overall, our data indicate that I119 and I125 contribute directly to the formation of the helicase–primase complex, whereas E15 and Y88 may mediate allosteric effects of other replisomal proteins on the helicase–primase complex (see Discussion).

Mutations in the C-domain of DnaB

Previous studies with truncated derivatives and mutants of *E.coli* DnaB concluded that the D212A-D213A and K216A-K217A double mutants are defective in DnaG binding and DnaG priming on M13 ssDNA (27). Although these residues are not conserved in T7 gp4 (30,31,39) and RepA helicases, sequence comparisons revealed that the equivalent residues in T7 gp4 (T293, G294 and D297, K298) and RepA (P18, P19 and Y22, V23) are situated on the outside of the ring in the crystal structures and could potentially interact with DnaG (Supplementary Material). Similar sequence comparisons with our *B.stearothermophilus* DnaB revealed that the equivalent residues (T191, E192 and R195, M196) are in the C-domain (26), and a simple structural comparison based upon the T7 gp4 crystal structure revealed that these residues are also situated on the outside periphery of the ring, potentially forming an interaction interface with the primase (Supplementary Material). To test this we constructed the T191A-E192A and R195A-M196A double mutants and tested their interaction with DnaG in a similar manner to the N-domain and linker mutants described above. Both mutants behaved just like the wild-type DnaB protein. They formed stable complexes with DnaG under low and high ionic strength conditions, and their ATPase and helicase activities were stimulated by DnaG (Supplementary Material). We conclude that these residues are not involved in the primase interaction. However, we should emphasize that the amino acid sequence homology between the *E.coli* and *B.stearothermophilus* DnaB proteins is not good in this region and it may be that other residues nearby may be involved instead. In order to test this possibility and also whether the C- and N-domains interact transiently with DnaG we utilized the Y2H methodology (see below).

The N- and C-domains of DnaB do not interact with DnaG

Bacillus stearothermophilus DnaB has a two-domain organization similar to that of *E.coli* DnaB (26). Sequence comparisons have identified a potential domain boundary that is very close to the domain boundary identified by our limited proteolysis studies (see below) and the two domains have been cloned, overexpressed and purified (19). Despite the fact that full-length DnaB forms a tight complex with DnaG (or P16), neither of the domains either alone or in a mixture formed a tight complex with DnaG (19). However, the possibility that DnaG interacts transiently with the N- and C-domains of DnaB has not been investigated. We examined these potential interactions by Y2H experiments. The interaction between DnaB and DnaG revealed a strong signal, but neither the N- nor the C-domains of DnaB revealed significant signals to suggest even a transient interaction with DnaG (Fig. 3). In agreement with our mutagenesis experiments, these data also suggest that the presence of an intact linker region that connects the N- and C-domains of DnaB is crucial for its interaction with DnaG. Any potential primase-interacting residues on either the N- or C-domain of DnaB do not contribute the main binding energy of this interaction. The direct involvement of the linker region was confirmed by limited proteolysis protection studies.

Primase-mediated protection of the linker region from limited proteolysis

The domain organization of *B.stearothermophilus* DnaG is similar to that of *E.coli* DnaG (19). A 16 kDa C-terminal domain (P16) is sufficient to bind stably to DnaB and stimulate its ATPase and helicase activities (19). We argued that if P16 binds to the flexible linker, then it should protect it from proteolytic cleavage. We proceeded to examine proteolytic fragments of DnaB in the presence and absence of P16 (Fig. 4). Our initial studies with trypsin revealed that P16 could be cleaved readily into a smaller fragment ($P16_N$) with its N-terminal sequence identical to that of the full-length P16 (Fig. 4a). Trypsin also appeared to cleave DnaB within the flexible linker region but at multiple closely spaced sites, making precise determination of these sites impossible (Fig. 4a and data not shown). Despite these complications, protection of the linker region in the presence of P16 was clearly evident in the first 5–10 min (compare gels in Fig. 4a in the presence and absence of P16), but as P16 was cleaved by trypsin to a smaller fragment protection was rapidly lost. These data imply indirectly that P16 itself comprises of two subdomains with only its C-terminal subdomain interacting with DnaB. This subdomain is sensitive to multiple trypsin cleavages and its extensive digestion with time (10–25 min) abolishes the interaction with DnaB. The NMR solution structure of P16 will confirm this (our collaboration with J. Waltho, University of Sheffield, UK, in preparation).

Papain produced clearer results as it did not digest P16 and also cleaved within the linker region at a defined site (Fig. 4b). Papain also cleaved ~10 kDa from the C-terminus of DnaB (C2d fragment), leaving a shorter version of DnaB including domains Nd and C1d (Fig. 4b). We were not able to identify this internal papain cleavage site. The site within the linker region was identified between two arginines within the 115-LRRL-118 sequence that is situated 38 residues closer to the N-terminus than the putative trypsin cleavage site identified by sequence comparisons (26). The LRRL site is just before one of our target residues (I119) and it is likely to be at the very beginning of the flexible region that connects the N- and C-terminal domains of DnaB (Supplementary Material). In the presence of P16 this site was protected from papain cleavage, as manifested by the relative resistance of the Nd/C1d

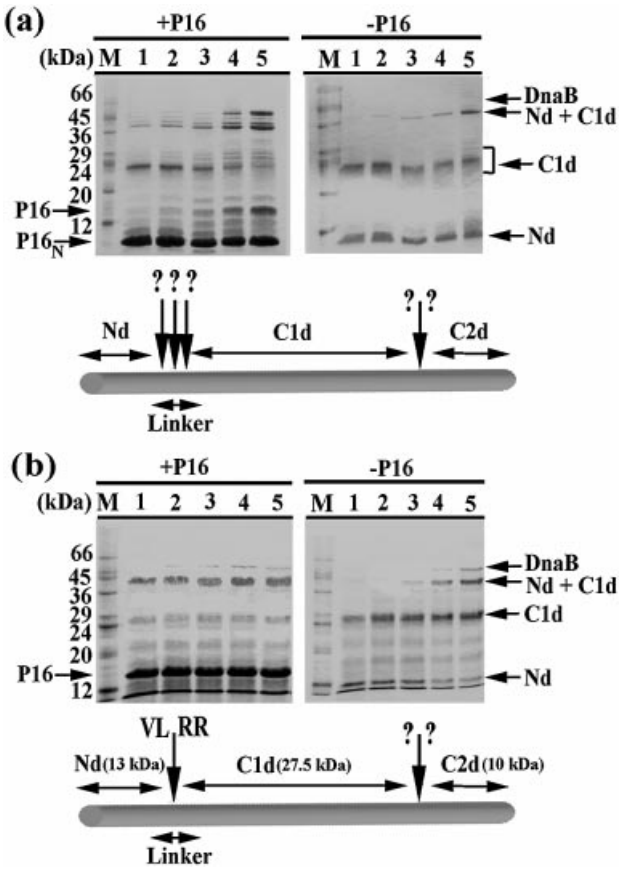

Figure 4. Protection of the linker region from limited proteolysis. Time course reactions of (**a**) papain and (**b**) trypsin digestions of DnaB in the presence and absence of P16, as indicated. Lanes represent molecular weight standards (M) and 25, 20, 15, 10 and 5 min of digestion from lanes 1–5, respectively. A schematic diagram at the bottom indicates the proteolytic sites and the domains resolved (Nd, C1d and C2d) with their approximate sizes. The relative position of the linker is also indicated. Arrows indicate the positions of all the DnaB domains and the P16 protein in the gels, for clarity. The proteolytic site between domains C1d and C2d could not be identified. Trypsin cleaved within the linker region at multiple sites as indicated, which could not be identified individually. Trypsin also cleaved P16 into a smaller fragment ($P16_N$) as indicated, with its N-terminal sequence being identical to that of full-length P16.

fragment to papain treatment, compared with its quick disappearance and the appearance of the C1d and Nd fragments in the absence of P16 (Fig. 4b). Overall, our data present direct evidence that P16 binds across the flexible linker region between the N- and C-terminal domains of DnaB. Furthermore, P16 itself comprises of two subdomains with its C-terminal subdomain being responsible for the interaction with DnaB.

The DnaB–DnaG complex adopts a 3-fold symmetric structure

Taking advantage of the stability of the *B.stearothermophilus* DnaB–DnaG complex, we attempted to elucidate its architecture by AFM. Imaging of DnaB alone in this and in our previous studies revealed polymorphic rings with 3-fold, 6-fold and open-ring structures, as well as smaller non-circular structures representing various oligomeric forms of dissociated DnaB monomers (15). However, 6-fold symmetric

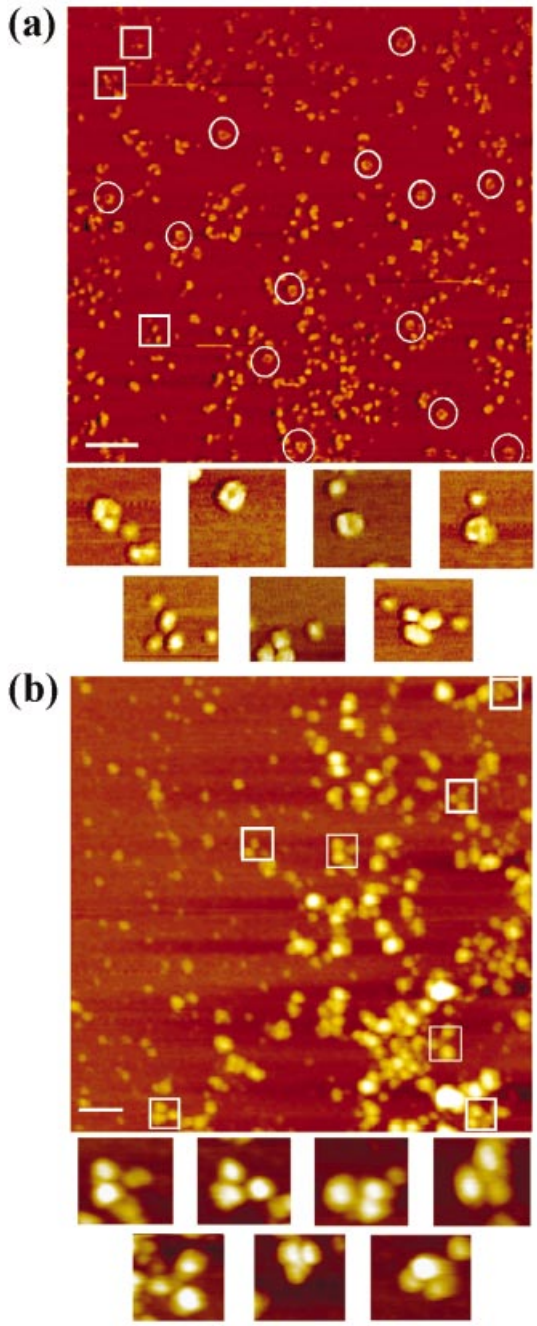

Figure 5. AFM images of the DnaB–DnaG complex obtained in topography mode. Representative field views from (**a**) imaging experiments of DnaB alone and (**b**) the purified DnaB–DnaG complex. Circles in the field views indicate some 6-fold symmetric rings whereas squares indicate 3-fold symmetric rings. The 6-fold symmetric rings are over-represented in DnaB samples, whereas the 3-fold symmetric rings are over-represented in DnaB–DnaG complex samples. Scale bars in the field views represent 100 nm. Representative samples from these ring structures are also shown at higher magnification below the field views.

rings were by far the largest number of structures visible (Fig. 5a and data not shown). Imaging of the purified complex revealed exclusively 3-fold symmetric rings compared with the DnaB alone (Fig. 5b). Measuring the mean dimensions of the three globular subunits that constitute the 3-fold symmetric ring in 18 different samples revealed that in the case of the

(a)

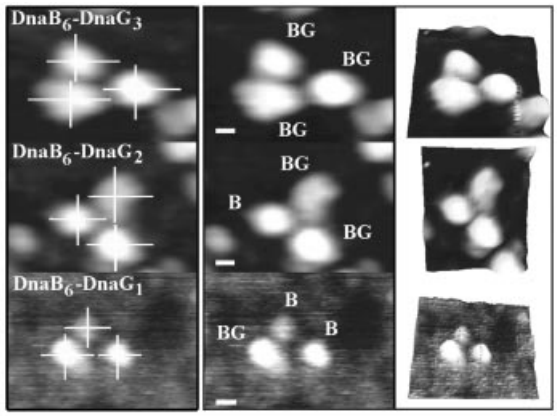

(b)

	X	Y		X_{BG}	Y_{BG}	X_B	Y_B
DnaB			$DnaB_6$-$DnaG_2$				
Mean (nm)	14.50	14.52	Mean (nm)	24.40	24.90	20.00	19.80
s.d.	2.48	2.75	s.d.	4.67	3.11	0.00	0.45
n	45	45	n	10	10	5	5
DnaG			$DnaB_6$-$DnaG_1$				
Mean (nm)	10.55	15.77	Mean (nm)	21.50	26.50	16.69	16.38
s.d.	3.01	2.91	s.d.	6.56	7.19	2.58	2.50
n	20	20	n	4	4	8	8
$DnaB_6$-$DnaG_3$							
Mean (nm)	26.11	25.14					
s.d.	5.00	4.96					
n	18	18					

Figure 6. The dimensions of the 3-fold symmetric DnaB–DnaG complex rings. (**a**) Representative 3-fold symmetric rings showing $DnaB_6$–$DnaG_3$, $DnaB_6$–$DnaG_2$ and $DnaB_6$–$DnaG_1$, as indicated. Each of the ring subunits was measured individually on both the *X* and *Y* axes, as shown. Scale bars represent 10 nm. The complexed DnaB–DnaG subunits of the ring are indicated as BG (a DnaB dimer bound to one DnaG molecule), whilst B indicates the DnaB subunits alone (a DnaB dimer). (**b**) The data from the analysis above. Sample sizes are indicated by the letter *n* and s.d. indicates standard deviation. Images of DnaG revealed monomeric structures (data not shown) whose dimensions were also measured in a similar manner. Data from the $DnaB_6$–$DnaG_2$ and $DnaB_6$–$DnaG_1$ complexes are subdivided into X_{BG}, Y_{BG} for the complexed DnaB–DnaG subunits and X_B, Y_B for the DnaB subunits. All images shown have been obtained in topography mode.

complex they were 26.1 ± 5.0 nm and 25.1 ± 5.0 nm along the *X* and *Y* axes, respectively (Fig. 6). By comparison, the equivalent mean dimensions of these subunits in 45 different samples of DnaB alone were 14.5 ± 2.5 nm (*X* axis) and 14.5 ± 2.8 nm (*Y* axis) (Fig. 6). Similar measurements of DnaG monomeric images in 20 different samples revealed a structure of mean dimensions 10.6 ± 3.0 nm (*X* axis) by 15.8 ± 2.9 nm (*Y* axis) (Fig. 6 and data not shown). These data indicate that the dimensions of the complex are approximately equal to the dimensions of the DnaB ring alone plus the dimensions of the globular DnaG monomer. We should emphasize that the DnaB–DnaG complexes used in our imaging experiments were purified by gel filtration and were not simple mixtures of individual DnaB and DnaG proteins (see Materials and Methods). Although the spatial resolution was not high enough to resolve individual subunits within the complex, collectively our data indicate that the complex adopts a 3-fold symmetric structure, compared with DnaB alone which adopts a variety of ring conformations with the 6-fold symmetrical rings clearly over-represented in this mixed population of structures (Fig. 5). Whether DnaG binds only to 3-fold symmetric DnaB rings or also to 6-fold rings, converting them to 3-fold rings, is not known. Despite the fact that our sample sizes (*n*) were not very large and that other non-circular structures were also visible in field views of the complex, possibly representing dissociated DnaB and DnaG proteins, this pattern was very reproducible in many different imaging experiments. We interpret these data as three molecules of DnaG bound around the outside perimeter of a 3-fold symmetric DnaB ring ($DnaB_6$–$DnaG_3$). Closer inspection of the complex rings revealed that although the majority of rings appeared to represent $DnaB_6$–$DnaG_3$ structures, a few complexes also appeared to represent $DnaB_6$–$DnaG_2$ and $DnaB_6$–$DnaG_1$ complexes with one or two DnaG molecules, respectively, bound to the DnaB hexamer (Fig. 6 and data not shown). We analysed nine such complexes and found that five of them were potentially $DnaB_6$–$DnaG_2$ while the other four were $DnaB_6$–$DnaG_1$ (Fig. 6). Because of the small sample sizes we can only speculate about the potential presence of a small amount of complexes with stoichiometries other than $DnaB_6$–$DnaG_3$. Whether such complexes exist *in vivo* and their biological relevance remain to be investigated in more detail. Overall our data suggest a speculative model for the architecture of the helicase–primase complex (see Discussion).

DISCUSSION

The importance of the helicase–primase interaction in DNA replication

DnaG is an essential enzyme for DNA synthesis (40). Its function is to initiate (prime) DNA synthesis as a consequence of the inability of DNA polymerases to initiate DNA synthesis *de novo* (23,25). While synthesis of the leading strand is achieved in a 'continuous' reaction that requires only one priming event by the DNA primase, synthesizing the complementary lagging strand is more problematic and involves a series of 'discontinuous' reactions, each requiring its own priming event.

The mode of action of the primase on the lagging strand during DNA replication is believed to be distributive. DnaB associates transiently with the primase and introduces it to the replication fork, while at the same time activating its priming activity. Once the RNA primer is synthesized, the primase will remain adhered tightly to the primed site, preventing primer dissociation and protecting it from nucleases and against action by DNA polymerases other than the main replicative DNA polymerase III (41). The association of the primase with the primed site is the result of a protein–protein interaction between the single-strand-binding (SSB) protein bound near the primed site and the primase (41). The removal of the primase from the priming site signifies the switch from priming to polymerization and is mediated by the χ subunit of the clamp loader (γ complex). The χ subunit of the γ complex competes with the primase for SSB and displaces it from the primed site (41).

The architecture of the helicase–primase interaction

The helicase–primase interaction involves two or three primase molecules per helicase hexamer (19). The 16 kDa C-terminal domain (P16) of the primase interacts with the helicase and is sufficient to elicit maximal stimulation of DnaB activity (18,19). The structures of the N-terminal

domain P12 (42) and the core central polymerization domain (43) of DnaG have been solved previously. The region of DnaB that interacts with P16 is not known and is currently the subject of much debate. Mutagenesis studies combined with indirect biochemical assays have revealed potential interaction interfaces in both the N-terminal (23) and C-terminal (27) domains of DnaB as well as within the flexible linker region that connects these domains (25). At first glance these data appear incompatible, as speculative comparisons with the T7 gp4 hexameric helicase suggest that the C-domain residues are unlikely to be part of the primase-interacting pocket. These residues are likely to be situated near the C-terminal face of the ring away from the N-terminal face (23). However, our comparisons with the RepA crystal structure (32) revealed that although the equivalent residues in RepA are indeed closer to the C-terminal face of the ring, they are also spatially close to the N-terminus and could participate in an extensive primase interacting interface that spans regions of the C- and N-domains as well as the linker region in between. Obviously this extensive interface will be defined by the spatial orientation of the N-domain relative to the C-domain. The flexibility of the N-domains within the ring has been highlighted recently in the *E.coli* DnaB where three of these domains interact with neighbouring C-domains within 3-fold symmetric rings (38).

Studies so far have been handicapped by the instability of the DnaB–DnaG complex *in vitro* and our inability to assay this interaction directly. Indirect assays cannot differentiate between DnaB mutations that directly affect this interaction and those that do not but are functional mutations (affect ATPase and/or helicase activities). For example, we have shown previously that K216A and Q362K mutations in the active site of *B.stearothermophilus* DnaB do not affect direct binding to P16 but abolish the P16-mediated stimulatory effect on the ATPase activity (33). Equally, the E241A mutation results in a protein with an ATPase activity stimulated by P16 binding but with no helicase activity (33). Such functional mutations will still appear as primase interacting deficient in indirect assays. The *B.stearothermophilus* system provides a very stable helicase–primase complex and allows direct investigation of this interaction. Both the primase and helicase in this system have domain organizations comparable to their *E.coli* counterparts (19). They also share significant sequence homologies (30% identity, 50% similarity for DnaG, and 45% identity, 69% similarity for DnaB), suggesting a close structural/functional relationship. Although the *B.stearothermophilus* DnaB–DnaG complex is very stable, no stable interaction could be detected between the primase and either of the N- and C-terminal domains of the helicase (19). In this paper we have shown that even a transient interaction between either of the two DnaB domains with DnaG could not be detected. The inability of the primase to form stable complexes with any of the individual helicase domains suggests that either the interaction interface includes residues from both domains or that it involves the linker region between these domains.

Taking advantage of the stability of the helicase–primase complex in *B.stearothermophilus* we reviewed all available mutagenesis data from other systems and tested them in our system, providing direct evidence that the primase interacts mainly with the flexible linker region connecting the N- and C-terminal domains of the helicase. Residues such as Y88 that are present on the N-domain are likely to modulate subtle functional aspects rather than provide the main binding energy of this interaction.

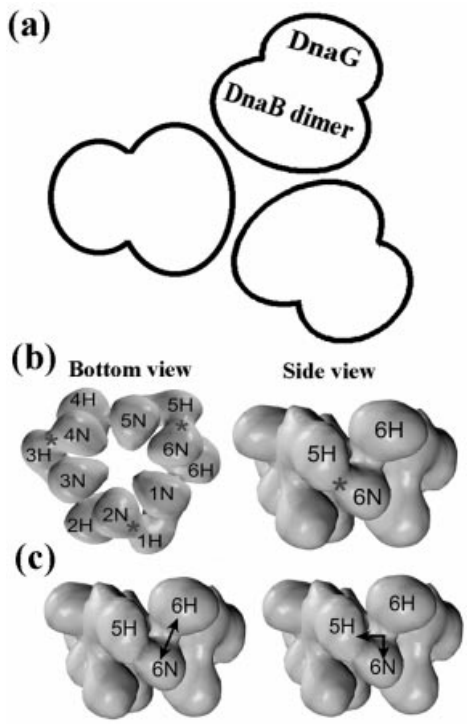

Figure 7. A speculative model for the architecture of the DnaB–DnaG complex. (**a**) A schematic model showing the 3-fold symmetric architecture of the helicase–primase complex. The six monomers of the helicase adopt a 3-fold (trimer of dimers) geometry with three primase molecules bound around the outside periphery of the ring. (**b**) The architecture of the 3-fold hexameric *E.coli* DnaB ring, viewed along the 3-fold symmetry axis (bottom view) and perpendicular to the axis (side view). The N- and C-(helicase) domains of adjacent monomers that constitute the three dimers around the ring are labelled for clarity. Asterisks indicate the interacting N- and C-domains of adjacent monomers. (**c**) Side views of the 3-fold symmetric ring. Double arrows indicate two possible ways that a molecule of DnaG could interact with one of the DnaB dimers of the ring. DnaG could interact with either one subunit (6N-linker-6H) or both subunits of the dimer (6N-linker-5H). Panels (b) and (c) were kindly provided by Ed Egelman (38).

Our AFM data revealed that the complex adopts a 3-fold symmetric ring structure, allowing us to speculate about its possible architecture. We suggest that the complex is arranged around a 3-fold (trimer of dimers) symmetric DnaB ring, with one DnaG monomer per dimer of DnaB arranged around the outside periphery of the ring (Fig. 7a). The DnaB-interacting P16 domain of DnaG interacts with the linker region between the N- and C-domains of either the same DnaB monomer or adjacent monomers of the ring. The orientation of the rest of the DnaG molecule relative to the DnaB ring is not known. The most likely position of the rest of the DnaG molecule (including the zinc-binding and polymerization domains) is in the vicinity of the rear of the DnaB ring (N-terminal face), ideally situated to interact with the ssDNA as it emerges from the ring of the forward-moving helicase. Whether the primase active site faces outward from the central hole, as is the case in T7 gp4 helicase–primase (44), or inward towards the central

hole, as suggested for the *E.coli* DnaG (43), is not clear at present. Both orientations could be accommodated in our model.

Recent electron microscopy studies of the *E.coli* DnaB protein revealed dynamic interactions of the N- and C-domains around the ring, with the N-domain of alternating monomers interacting with the C-domains of neighbouring monomers around the 3-fold symmetric ring (38) (Fig. 7b). Such an architectural arrangement would imply that the primase could interact across the flexible linker with the N- and C-domains of the same DnaB monomer or alternatively across the N- and C-domains of neighbouring monomers as shown in Figure 7c. Our model predicts three primase molecules per hexamer and mechanistically is consistent with the F1-ATPase-based helicase mechanism (45) rather than the proposed sequential mechanism based upon a crystal structure of the T7 helicase that shows effectively a pair of trimers forming a ring (31). Having said that, our data also revealed a small number of complexes with stoichiometries $DnaB_6$–$DnaG_2$ and $DnaB_6$–$DnaG_1$. The biological relevance (if any) of these complexes is not clear at present, but a $DnaB_6$–$DnaG_2$ complex is consistent with the sequential mechanism rather than the F1-ATPase-based helicase mechanism. Although this is a good starting model, albeit speculative, the precise molecular details of the helicase–primase interaction await the solution of the crystal structure of the DnaB–DnaG complex.

SUPPLEMENTARY MATERIAL

Supplementary Material is available at NAR Online.

ACKNOWLEDGEMENTS

The authors thank Kevin Bailey for N-terminal protein sequencing and Christopher Anderson with help on the AFM. This work was supported by the BBSRC (42/B15519 grant to P.S. and 42/E12956 to C.J.T.). J.T. and I.J.T. are postgraduate students, supported by a University of Nottingham Research Scholarship and BBSRC, respectively. Ed Egelman provided Figure 7b and c.

REFERENCES

1. Caruthers,J.M. and McKay,D.B. (2002) Helicase structure and mechanism. *Curr. Opin. Struct. Biol.*, **12**, 123–133.
2. von Hippel,P.H. and Delagoute,E. (2001) A general model for nucleic acid helicases and their 'coupling' within macromolecular machines. *Cell*, **104**, 177–190.
3. Soultanas,P. and Wigley,D.B. (2000) DNA helicases: 'inching forward'. *Curr. Opin. Struct. Biol.*, **10**, 124–128.
4. Patel,S.S. and Picha,K.M. (2000) Structure and function of hexameric helicases. *Annu. Rev. Biochem.*, **69**, 651–697.
5. Katayama,T., Kubota,T., Kurokawa,K., Crooke,E. and Sekimizu,K. (1998) The initiator function of DnaA protein is negatively regulated by the sliding clamp of the *E.coli* chromosomal replicase. *Cell*, **94**, 61–71.
6. Datta,H.J., Khatri,G.S. and Bastia,D. (1999) Mechanism of recruitment of DnaB helicase to the replication origin of the plasmid pSC101. *Proc. Natl Acad. Sci. USA*, **96**, 73–78.
7. Konieczny,I. and Marszalek,J. (1995) The requirement for molecular chaperones in lambda-DNA replication is reduced by the mutation-Pi in lambda-P gene, which weakens the interaction between lambda-P protein and DnaB helicase. *J. Biol. Chem.*, **270**, 9792–9799.
8. Wahle,E., Lasken,R.S. and Kornberg,A. (1989) The dnaB–dnaC replication protein complex of *Escherichia coli*. I. Formation and properties. *J. Biol. Chem.*, **264**, 2463–2468.
9. Wahle,E., Lasken,R.S. and Kornberg,A. (1989) The dnaB-dnaC replication protein complex of *Escherichia coli*. II. Role of the complex in mobilizing dnaB functions. *J. Biol. Chem.*, **264**, 2469–2475.
10. Imai,Y., Ogasawara,N., Ishigo-Oka,D., Kadoya,R., Daito,T. and Moriya,S. (2000) Subcellular localization of DNA-initiation protein of *Bacillus subtilis*: evidence that chromosome replication begins at either edge of the nucleoids. *Mol. Microbiol.*, **36**, 1037–1048.
11. Soultanas,P. (2002) A functional interaction between the putative primosomal protein DnaI and the main replicative DNA helicase DnaB in *Bacillus*. *Nucleic Acids Res.*, **30**, 966–974.
12. Smelkova,N. and Marians,K.J. (2001) Timely release of both replication forks from oriC requires modulation of origin topology. *J. Biol. Chem.*, **276**, 39186–39191.
13. Kim,S., Dallmann,H.G., McHenry,C.S. and Marians,K.J. (1996) Coupling of a replicative polymerase and helicase: a τ-DnaB interaction mediates rapid replication fork movement. *Cell*, **84**, 643–650.
14. Haroniti,A., Till,R., Smith,M.C.M. and Soultanas,P. (2003) The clamp-loader-helicase interaction in *Bacillus*. Leucine 381 is critical for pentamerisation and helicase-binding of the *Bacillus* τ protein. *Biochemistry*, **42**, 10955–10964.
15. Haroniti,A., Anderson,C., Doddridge,Z., Gardiner,L., Roberts,C.J., Allen,S. and Soultanas,P. (2004) The clamp-loader-helicase interaction in *Bacillus*. Atomic force microscopy reveals the structural organization of the τ-DnaB complex in *Bacillus*. *J. Mol. Biol.*, **336**, 381–393.
16. Bussiere,D.E., Bastia,D. and White,S.W. (1995) Crystal-structure of the replication terminator protein from *Bacillus-subtilis* at 2.6-angstrom. *Cell*, **80**, 651–660.
17. Gautam,A., Mulugu,S., Alexander,K. and Bastia,D. (2001) A single domain of the replication termination protein of *Bacillus subtilis* is involved in arresting both DnaB helicase and RNA polymerase. *J. Biol. Chem.*, **276**, 23471–23479.
18. Tougu,K and Marians,K.J. (1996) The interaction between helicase and primase sets the replication fork clock. *J. Biol. Chem.*, **271**, 21391–21397.
19. Bird,L.E., Pan,H., Soultanas,P. and Wigley,D.B. (2000) Mapping protein–protein interactions within a stable complex of DNA primase and DnaB helicase from *Bacillus stearothermophilus*. *Biochemistry*, **39**, 171–182.
20. Ng,J.Y. and Marians,K.J. (1996) The ordered assembly of the ΦX174-type primosome. I. Isolation and identification of intermediate protein–DNA complexes. *J. Biol. Chem.*, **271**, 15642–15648.
21. Ng,J.Y and Marians,K.J. (1996) The ordered assembly of the ΦX174-type primosome. II. Preservation of primosome composition from assembly through replication. *J. Biol. Chem.*, **271**, 15649–15655.
22. Liu,J., Nurse,P. and Marians,K.J. (1996) The ordered assembly of the ΦX174-type primosome. III. PriB facilitates complex formation between PriA and DnaT. *J. Biol. Chem.*, **271**, 15656–15661.
23. Chang,P. and Marians,K.J. (2000) Identification of a region of *Escherichia coli* DnaB required for functional interaction with DnaG at the replication fork. *J. Biol. Chem.*, **275**, 26187–26195.
24. Maurer,R. and Wong,A. (1988) Dominant-lethal mutations in the dnaB helicase gene of *Salmonella typhimurium*. *J. Bacteriol.*, **170**, 3682–3688.
25. Stordal,L. and Maurer,R. (1996) Defect in general priming conferred by linker region mutants of *Escherichia coli* DnaB. *J. Bacteriol.*, **178**, 4620–4627.
26. Bird,L.E. and Wigley,D.B. (1999) The *Bacillus stearothermophilus* replicative helicase: cloning, overexpression and activity. *Biochim. Biophys. Acta*, **1444**, 424–428.
27. Lu,Y.B., Ratnakar,P., Mohanty,B.K. and Bastia,D. (1996) Direct physical interaction between DnaG primase and DnaB helicase of *Escherichia coli* is necessary for optimal synthesis of primer RNA. *Proc. Natl Acad. Sci. USA*, **93**, 12902–12907.
28. Fass,D., Bogden,C.E. and Berger,J.M. (1999) Crystal structure of the N-terminal domain of the DnaB hexameric helicase. *Structure*, **7**, 691–698.
29. Weigelt,J., Brown,S.E., Miles,C.S., Dixon,N.E. and Otting,G. (1999) NMR structure of the N-terminal domain of *E.coli* DnaB helicase: implications for structure rearrangements in the helicase hexamer. *Structure*, **7**, 681–690.

30. Sawaya,M.R., Guo,S., Tabor,S., Richardson,C.C. and Ellenberger,T. (1999) Crystal structure of the helicase domain from the replicative helicase–primase of bacteriophage T7. *Cell*, **99**, 167–177.
31. Singleton,M.R., Sawaya,M.R., Ellenberger,T. and Wigley,D.B. (2000) Crystal structure of T7 gene 4 ring helicase indicates a mechanism for sequential hydrolysis of nucleotides. *Cell*, **101**, 589–600.
32. Niedenzu,T., Roleke,D., Bains,G., Scherzinger,E. and Saenger,W. (2001) Crystal structure of the hexameric replicative helicase RepA of plasmid RSF1010. *J. Mol. Biol.*, **306**, 479–487.
33. Soultanas,P. and Wigley,D.B. (2002) Site-directed mutagenesis reveals roles for conserved amino acid residues in the hexameric DNA helicase DnaB from *Bacillus stearothermophilus*. *Nucleic Acids Res.*, **30**, 4051–4060.
34. Pullman,M.E., Penefsky,A., Datta,A. and Racker,E. (1960) Partial resolution of the enzymes catalysing oxidative phosphorylation. *J. Biol. Chem.*, **235**, 3322–3329.
35. Becker,D.M. and Guarente,L. (1991) High-efficiency transformation of yeast by electroporation. *Methods Enzymol.*, **194**, 182–187.
36. Dumay,H., Rubbi,L., Sentenac,A. and Marck,C. (1999) Interaction between yeast RNA polymerase III and transcription factor TFIIIC via ABC10α and τ131 subunits. *J. Biol. Chem.*, **274**, 33462–33468.
37. Biswas,S.B., Chen,P.H. and Biswas,E.E. (1994) Structure and function of *Escherichia coli* DnaB protein: role of the N-terminal domain in helicase activity. *Biochemistry*, **33**, 11307–11314.
38. Yang,S., Yu,X., VanLoock,M.S., Jezewska,M.J., Bujalowski,W. and Egelman,E.H. (2002) Flexibility of the rings: structural asymmetry in the DnaB hexameric helicase. *J. Mol. Biol.*, **321**, 839–849.
39. Bird,L.E., Hakansson,K., Pan,H. and Wigley,D.B. (1997) Characterisation and crystallisation of the helicase domain of bacteriophage T7 gene 4 protein. *Nucleic Acids Res.*, **25**, 2620–2626.
40. Frick,D.N. and Richardson,C.C. (2001) DNA primases. *Annu. Rev. Biochem.*, **70**, 39–80.
41. Yuzhakov,A., Kelman,Z. and O'Donnell,M. (1999) Trading places on DNA—a three-point switch underlies primer handoff from primase to the replicative DNA polymerase. *Cell*, **96**, 153–163.
42. Pan,H. and Wigley,D.B. (2000) Structure of the zinc-binding domain of *Bacillus stearothermophilus* DNA primase. *Structure*, **8**, 231–239.
43. Keck,J.L., Roche,D.D., Lynch,A.S. and Berger,J.M. (2000) Structure of the RNA polymerase domain of *E.coli* primase. *Science*, **287**, 2482–2486.
44. Van Loock,M.S., Chen,Y.-J., Yu,X., Patel,S.S. and Egelman,E.H. (2001) The primase active site is on the outside of the hexameric bacteriophage T7 gene 4 helicase–primase ring. *J. Mol. Biol.*, **311**, 951–956.
45. Hingorani,M.M., Washington,M.T., Moore,K.C. and Patel,S.S. (1996) The dTTPase mechanism of T7 DNA helicase resembles the binding change mechanism of the F1-ATPase. *Proc. Natl Acad. Sci. USA*, **94**, 5012–5017.